

# Many-body Quantum Geometry in Superconductor-Quantum Dot Chains

R. L. Klees,<sup>1</sup> J. C. Cuevas,<sup>2</sup> W. Belzig,<sup>1</sup> and G. Rastelli<sup>1,3</sup>

<sup>1</sup>*Fachbereich Physik, Universität Konstanz, D-78457 Konstanz, Germany*

<sup>2</sup>*Departamento de Física Teórica de la Materia Condensada and Condensed Matter Physics Center (IFIMAC), Universidad Autónoma de Madrid, E-28049 Madrid, Spain*

<sup>3</sup>*Zukunftskolleg, Universität Konstanz, D-78457 Konstanz, Germany*

(Dated: September 25, 2020)

Multiterminal Josephson junctions constitute engineered topological systems in arbitrary synthetic dimensions defined by the superconducting phases. Microwave spectroscopy enables the measurement of the quantum geometric tensor, a fundamental quantity describing both the quantum geometry and the topology of the emergent Andreev bound states in a unified manner. In this work we propose an experimentally feasible multiterminal setup of  $N$  quantum dots connected to  $N + 1$  superconducting leads to study nontrivial topology in terms of the many-body Chern number of the ground state. Moreover, we generalize the microwave spectroscopy scheme to the multiband case and show that the elements of the quantum geometric tensor of the noninteracting ground state can be experimentally accessed from the measurable oscillator strengths at low temperature.

## I. INTRODUCTION

The concept of topology plays an important role in modern branches of theoretical physics by explaining the quantized nature of certain physical phenomena. The pursuit to find novel types of topologically nontrivial systems providing quantized observables classified by integers has created a new research field called topological band theory [1]. Since then, a huge variety of topological quantum matter has been predicted and discovered such as topological insulators [2, 3], topological semimetals [4], topological superconductors [5], as well as non-Hermitian (e.g., open/dissipative) topological systems [6]. Out of these, the superconducting systems are also promising platforms for topologically protected quantum computation which relies on non-Abelian exchange statistics, i.e., braiding, of Majorana zero modes appearing at the Fermi energy [7–9] and their appearance was recently verified experimentally [10]. Furthermore, qubits based on the Andreev bound states (ABS) appearing inside a Josephson junction have also been proposed [11, 12]. These bound states can be experimentally accessed and coherently manipulated by microwave [13–16], tunneling [17], and supercurrent spectroscopy [18] if the junction is embedded in an rf superconducting quantum interference device (SQUID).

More recently, multiterminal Josephson junctions (MJJs) consisting of many superconducting terminals have been theoretically investigated and shown to exhibit topologically nontrivial physics [19–29, 32–34]. In such multiterminal systems, topology emerges in the synthetic space of superconducting phases and the integer-valued Chern number can manifest itself in a quantized transconductance between two terminals [22, 24–31]. The advantage of these systems is that, in principle, an arbitrary number of synthetic dimensions can be implemented by simply increasing the number of superconducting leads and that building blocks can be conventional materials, although also topological superconductors hosting Majorana zero modes have been studied

in this context [29–31]. Moreover, it has been recently suggested to use microwave spectroscopy to measure the more fundamental quantum geometric tensor of ABS, which provides both the information about the geometry of the state manifold and the topological information contained in the Berry curvature [32]. While the Chern number follows directly from the local Berry curvature by a simple integration, the local metric tensor carries important information on, for instance, energy fluctuations and the noise spectral function [35, 36], as well as quantum phase transitions [37] and wave packet dynamics [38–40]. Finally, it is also possible to strongly drive topologically trivial Josephson systems to eventually generate nontrivial (Floquet) topology [41, 42].

So far, many experiments to measure quantum geometry (i.e., the Berry curvature and/or the quantum metric) and the related topology have already been successfully carried out in, e.g., ultracold fermionic atoms [43, 44], superconducting qubits and qutrits [45, 46], superconducting transmon qubits [47], superconducting quantum circuits [48], qubits in NV centers in diamond [49], high-finesse planar microcavities [50], and coupled fiber loops [51].

Additional interesting directions are topological fermion-parity [52] and Cooper-pair pumps [53–58] in which Weyl singularities in parameter space are responsible for a quantized adiabatic transfer of single charges (charge  $1e$ ) and Cooper pairs (charge  $2e$ ), respectively.

Although recently a diffusive three-terminal MJJ in a double-SQUID configuration has been both experimentally and theoretically investigated on its topological real-space properties [59] followed by a detailed theoretical study [60], it is still challenging to create MJJs [17, 61]. Furthermore, despite the fact that first experiments towards ballistic MJJs have been performed [62, 63], the more general theoretical proposals of MJJs discussed above are expected to be quite challenging to realize since the necessary space for experimental control gates decreases as the number of superconducting terminals increases. Such circular arrangements of the

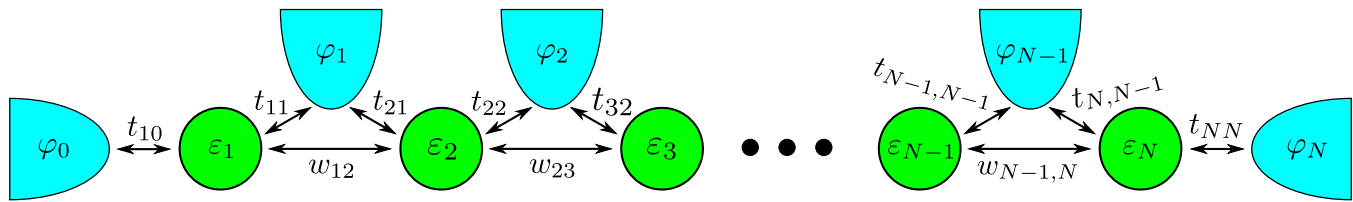


FIG. 1. Model of the superconductor-quantum dot chain. The chain consists of  $N$  quantum dots (each with onsite energy  $\varepsilon_j$ ,  $j = 1, \dots, N$ ) which are connected to  $N + 1$  s-wave superconducting leads (each with a pairing phase  $\varphi_k$ ,  $k = 0, \dots, N$ ). The couplings between the quantum dots are  $w_{l,l+1}$  ( $l = 1, \dots, N - 1$ ), while the couplings between the quantum dots and the superconducting leads are  $t_{j,j-1}$  and  $t_{jj}$ .

terminals will eventually have an adverse effect on the scalability of these systems.

In this work, we propose a linear design of an MJJ as an alternative and scalable device to study quantum geometry and topology in topological Josephson matter. This setup consists of a chain of quantum dots which are coupled to superconducting leads, as presented in Fig. 1. We think that this system is easier to realize and manipulate in experiments since there is enough space from below for additional necessary control gates and it could be implemented with already available ingredients such as carbon nanotubes or semiconducting nanowires contacted by superconductors [17, 64–68]. Moreover, we expect that it will be straightforward to extend the length of the chain and, hence, increase the number of dots and leads at will. We will show that such a system allows for the emergence of topologically nontrivial ABS and, therefore, represents an ideal platform to experimentally study quantum geometry and topology. We will also show how to apply microwave spectroscopy in such multiband systems to measure the quantum geometry of the noninteracting ground state (GS) as a whole, which is important for (quantized) quantum transport phenomena due to the collection of occupied single-particle states.

The rest of the paper is organized as follows: In Sec. II, we introduce and investigate the effective low-energy Hamiltonian of a linear chain of  $N$  dots coupled to  $N + 1$  superconductors. We also define the topological invariant of the many-body GS, i.e., the Chern number, and analyze the effects of the various parameters of this model on the topological phases of this system. In Sec. III, we discuss the application of microwave spectroscopy in such systems and show that, although the quantum geometry of the individual ABS is inaccessible at zero temperature, the GS topology and, more fundamentally, the GS quantum geometry can be accessed even in the multiband case. We discuss our findings and conclude our work in Sec. IV. Further details of derivations can be found in the Appendices A, B, and C.

## II. EFFECTIVE LOW-ENERGY MODEL AND TOPOLOGY

As described above, we start by considering a linear chain of  $N + 1$  BCS superconducting leads connected to  $N$  quantum dots as shown in Fig. 1. Each of the quantum dots is spin-degenerate with an onsite energy  $\varepsilon_j$  ( $j = 1, \dots, N$ ) and each s-wave superconductor has a pairing potential  $\Delta_k$  with a pairing phase  $\varphi_k$  ( $k = 0, \dots, N$ ). The dot  $j$  is coupled to two neighboring superconducting leads  $j - 1$  and  $j$  via the hoppings  $t_{j,j-1}$  and  $t_{jj}$ , respectively. To be more general, we include the effect of a direct tunneling between the dots without passing through the superconductors, which is described by a direct coupling  $w_{l,l+1}$  ( $l = 1, \dots, N - 1$ ) between the dots  $l$  and  $l + 1$ . By integrating out the subsystem of the superconducting leads and by considering the limit of large superconducting gaps  $\Delta_k \rightarrow \infty$ , we obtain an effective low-energy Hamiltonian describing the quantum dots proximity coupled to the superconductors. The derivation of the effective Hamiltonian of our model is presented in Appendix A.

The resulting Hamiltonian has the form  $H_{\text{eff}} = \mathbf{d}^\dagger \hat{H}_{\text{eff}}^{(N)} \mathbf{d}$ , where the  $2N \times 2N$  block-tridiagonal matrix Hamiltonian is given by

$$\hat{H}_{\text{eff}}^{(N)} = \begin{pmatrix} \hat{H}_1 & \hat{V}_{12} & 0 & \cdots & 0 & 0 \\ \hat{V}_{12} & \hat{H}_2 & \hat{V}_{23} & \cdots & 0 & 0 \\ 0 & \hat{V}_{23} & \hat{H}_3 & \cdots & 0 & 0 \\ \vdots & \vdots & \vdots & \ddots & \vdots & \vdots \\ 0 & 0 & 0 & \cdots & \hat{H}_{N-1} & \hat{V}_{N-1,N} \\ 0 & 0 & 0 & \cdots & \hat{V}_{N-1,N} & \hat{H}_N \end{pmatrix}, \quad (1)$$

which is written in the basis defined by the  $2N$ -dimensional Nambu spinor  $\mathbf{d}^\dagger = (d_{1\uparrow}^\dagger, d_{1\downarrow}, d_{2\uparrow}^\dagger, d_{2\downarrow}, \dots, d_{N\uparrow}^\dagger, d_{N\downarrow})$ , with  $d_{j\sigma}^{(\dagger)}$  being the annihilation (creation) operator of an electron with spin  $\sigma = \uparrow, \downarrow$  on the  $j$ -th dot. The  $2 \times 2$  Nambu blocks are given by

$$\hat{H}_j = \begin{pmatrix} \varepsilon_j & z_j \\ z_j^* & -\varepsilon_j \end{pmatrix}, \quad \hat{V}_{l,l+1} = \begin{pmatrix} w_{l,l+1} & z_{l,l+1} \\ z_{l,l+1}^* & -w_{l,l+1} \end{pmatrix}, \quad (2)$$

where the effective local and nonlocal proximity-induced

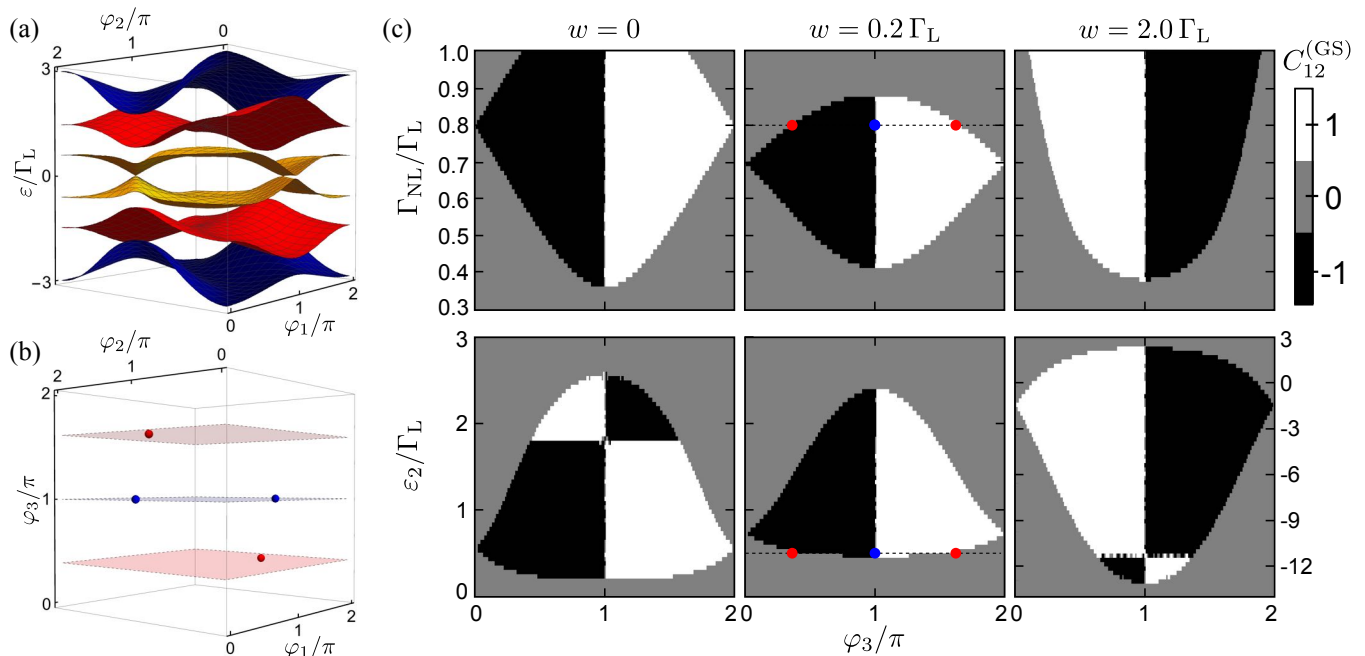


FIG. 2. (a) ABS energies  $\varepsilon_{A,-3}, \dots, \varepsilon_{A,3}$  (from bottom to top) for  $N = 3$  dots. Energy bands with the same color represent PH-symmetric ABS with energies  $\varepsilon_{A,\pm j}$ . Parameters:  $\varepsilon_1 = -\varepsilon_2 = \varepsilon_3 = -\Gamma_L/2$ ,  $\varphi_0 = 0$ ,  $\varphi_3 = \pi$ ,  $w = 0.2\Gamma_L$ ,  $\Gamma_{NL} = 0.8\Gamma_L$ . (b) Locations of the four Weyl points  $\varphi_W \in \mathbb{T}^3$  for which  $\varepsilon_{A,\pm 1}(\varphi_W) = 0$  for the same parameters as in panel (a). The color indicates the topological charge the Weyl points. The two blue Weyl points in the  $\varphi_3 = \pi$  plane are visible as zero-energy band crossings in panel (a). (c) Topological phase diagrams of the ground state Chern number  $C_{12}^{(GS)}$  for  $N = 3$  dots for different values of the direct tunneling  $w$  between the dots (columns) as a function of the phase  $\varphi_3$ . The upper row shows the phase diagram as a function of the nonlocal coupling  $\Gamma_{NL}$  for fixed  $\varepsilon_2 = \Gamma_L/2$ , while the lower row shows it as a function of the central dot level  $\varepsilon_2$  for fixed  $\Gamma_{NL} = 0.8\Gamma_L$ . All other parameters are the same as in panel (a). The dashed line with blue and red dots in the phase diagrams for  $w = 0.2\Gamma_L$  mark the locations of the planes with fixed  $\varphi_3$  in which the Weyl points of the same color appear in panel (b).

pairing potentials on the dots are defined as

$$z_j = \Gamma_j^{(j-1)} e^{i\varphi_{j-1}} + \Gamma_j^{(j)} e^{i\varphi_j}, \quad (3a)$$

$$z_{l,l+1} = \Gamma_{l,l+1}^{(l)} e^{i\varphi_l}, \quad (3b)$$

with  $\Gamma_j^{(k)} = \pi N_0 t_{jk}^2$  and  $\Gamma_{l,l+1}^{(l)} = \pi N_0 p t_{l,l+1}$ , respectively. In passing by, we modified the nonlocal pairings by a dimensionless factor  $p \in [0, 1]$  motivated by experiments in which typically  $\Gamma_{l,l+1}^{(l)} < \sqrt{\Gamma_l^{(l)} \Gamma_{l+1}^{(l)}}$  [66, 67]. This modification allows us to treat the nonlocal couplings as independent parameters from the local ones. In general, the parameter  $p$  modifying the nonlocal coupling  $\Gamma_{l,l+1}^{(l)}$  depends on the geometrical details of the contact as well as the coherence length of the Cooper pairs [69, 70].

Finally, as in a system of  $N + 1$  superconducting leads only  $N$  superconducting phases are independent, gauge-invariance allows us to set one of the superconducting phases to zero. We will consider  $\varphi_0 = 0$  in the following as a reference and the remaining  $N$  superconducting phases  $\varphi = (\varphi_1, \dots, \varphi_N) \in [0, 2\pi)^N$  define an  $N$ -dimensional periodic compact space  $\mathbb{T}^N$  ( $N$ -torus) in analogy to the quasimomenta in a periodic crystal with a first Brillouin zone.

For  $N$  quantum dots coupled to  $N + 1$  superconducting leads in the low-energy limit, there are  $2N$  ABS. Defining the sets of labels  $D^\pm = \{\pm 1, \dots, \pm N\}$  for occupied ( $D^-$ ) and empty ( $D^+$ ) states at zero temperature, the  $2N$  ABS  $|\psi_n\rangle$  ( $n \in D^- \cup D^+$ ) satisfy  $\hat{H}_{\text{eff}}^{(N)} |\psi_n\rangle = \varepsilon_{A,n} |\psi_n\rangle$ , where  $\varepsilon_{A,n}$  is the energy of the  $n$ -th ABS. In the following, we will consider the ABS being ordered as  $\varepsilon_{A,-N} \leq \dots \leq \varepsilon_{A,-1} \leq 0 \leq \varepsilon_{A,1} \leq \dots \leq \varepsilon_{A,N}$  without loss of generality.

The  $2N$  ABS come in  $N$  particle-hole (PH) symmetric pairs and fulfill  $|\psi_{-j}\rangle = P^{(N)} |\psi_j\rangle$  ( $j \in D^+$ ), where  $P^{(N)} = i(\mathbb{1}^{(N)} \otimes \tau_2)K$  is the operator of PH symmetry,  $K$  is complex conjugation,  $\mathbb{1}^{(N)}$  is the  $N \times N$  identity matrix, and  $\tau_2$  is the second Pauli matrix in Nambu space. Furthermore, the energies of a PH-symmetric pair are related by  $\varepsilon_{A,-j} = -\varepsilon_{A,j}$  since  $P^{(N)}$  satisfies the anti-commutation relation  $\{\hat{H}_{\text{eff}}^{(N)}, P^{(N)}\} = 0$ .

Due to the large number of parameters, we choose equal local couplings  $\Gamma_j^{(k)} = \Gamma_L$ , equal nonlocal couplings  $\Gamma_{l,l+1}^{(l)} = \Gamma_{NL}$ , and equal interdot couplings  $w_{l,l+1} = w$  for simplicity. As an example, we show the ABS for  $N = 3$  dots in Fig. 2(a), which also shows that this system allows for the appearance of Weyl singularities, i.e., points of degeneracy  $\varphi_W \in \mathbb{T}^3$  at which two energy

bands cross [Fig. 2(b)]. As we will see below, Weyl points for which  $\varepsilon_{A,\pm 1}(\varphi_W) = 0$  are responsible for topological phase transitions between regions of different values of the Chern number of the GS of the system.

The superconducting phases  $\varphi$  define  $N$  synthetic  $U(1)$  gauge fields for which we define gauge connection 1-forms  $\mathcal{A}^{(n)} = \sum_{\alpha=1}^N a_{\alpha}^{(n)} d\varphi_{\alpha}$  for each of the ABS  $|\psi_n\rangle$ , where  $a_{\alpha}^{(n)} = i \langle \psi_n | \partial_{\alpha} \psi_n \rangle$  is the (Abelian) Berry connection [71] and  $\partial_{\alpha} \equiv \partial / \partial \varphi_{\alpha}$ . The gauge-invariant curvature 2-form  $\mathcal{F}^{(n)}$  of the  $n$ -th single-particle state is defined as the exterior derivative of  $\mathcal{A}^{(n)}$ , i.e.,  $\mathcal{F}^{(n)} = d\mathcal{A}^{(n)} = (1/2) \sum_{\alpha,\beta=1}^N f_{\alpha\beta}^{(n)} d\varphi_{\alpha} \wedge d\varphi_{\beta}$ , where  $f_{\alpha\beta}^{(n)} = \partial_{\alpha} a_{\beta}^{(n)} - \partial_{\beta} a_{\alpha}^{(n)}$  is the (Abelian) Berry curvature [72]. Finally, the first Chern numbers of an ABS  $|\psi_n\rangle$  are calculated as

$$c_{\alpha\beta}^{(n)} = \frac{1}{2\pi} \int_0^{2\pi} \int_0^{2\pi} f_{\alpha\beta}^{(n)} d\varphi_{\alpha} d\varphi_{\beta}, \quad (4)$$

which are defined by an integration in the  $(\varphi_{\alpha}, \varphi_{\beta})$  subplane of the  $N$ -torus  $\mathbb{T}^N$ . Notice that, due to PH symmetry, we have  $a_{\alpha}^{(-j)} = -a_{\alpha}^{(j)}$  and, consequently,  $f_{\alpha\beta}^{(-j)} = -f_{\alpha\beta}^{(j)}$  and  $c_{\alpha\beta}^{(-j)} = -c_{\alpha\beta}^{(j)}$ . We use the numerical algorithm developed by Fukui, Hatsugai, and Suzuki in Ref. [73] for a stable and gauge-independent calculation of the Chern numbers.

As shown in Appendix B, the Chern number of the noninteracting many-body GS is simply given by the sum of all individual Chern numbers of the occupied single-particle states, i.e.,

$$C_{\alpha\beta}^{(\text{GS})} = \sum_{j \in D^-} c_{\alpha\beta}^{(j)}. \quad (5)$$

Notice that  $C_{\alpha\beta}^{(\text{GS})}$  only changes if there is a zero-energy crossing between the two PH-symmetric ABS  $|\psi_{-1}\rangle$  and  $|\psi_1\rangle$ . Although there are of course Weyl points for which other energy bands cross changing the individual Chern numbers from, e.g., 0 to  $\pm 1$ , the sum of them entering  $C_{\alpha\beta}^{(\text{GS})}$  in Eq. (5) will still be unchanged.

In order to obtain topologically nontrivial states in terms of  $C_{\alpha\beta}^{(\text{GS})}$ , the minimal number of quantum dots is  $N = 3$ . To analyze and discuss the stability the topological phases for this case, we show topological phase diagrams in Fig. 2(c) in terms of the GS Chern number  $C_{12}^{(\text{GS})}$ . We see that there are large and stable regions for which nontrivial regions of  $C_{12}^{(\text{GS})} \neq 0$  appear. This stability is due to the separation of Weyl points  $\varphi_W$  of different topological charge [Fig. 2(b)]. These Weyl points move continuously in  $\mathbb{T}^3$  while the parameters of the system are changed, making these regions robust against small fluctuations. As long as two Weyl points of different topological charge do not meet and annihilate, topological regions will be present. Interestingly, we see that it is not necessary that the quantum dots are directly coupled ( $w = 0$ ) for the Chern number to be nontrivial. For a

small coupling  $w = 0.2\Gamma_L$  we still find topologically nontrivial regions. Remarkably, a larger interdot coupling of  $w = 2\Gamma_L$  can also enhance the size of topological regions in parameter space, although the two regions of finite Chern number are interchanged. However, if the interdot coupling becomes too strong ( $w \gg \Gamma_L$ , not shown), topological regions completely disappear since the effect of the superconductors will be negligible. In addition, we see that the nonlocal couplings  $\Gamma_{\text{NL}}$  can be considerably smaller than the local couplings  $\Gamma_L$  and that there is a lot of freedom in experimental tunability of, e.g., the central dot level  $\varepsilon_2$ . For  $w = 2\Gamma_L$  and  $\Gamma_{\text{NL}} = 0.8\Gamma_L$ ,  $\varepsilon_2$  can be detuned even up to  $\varepsilon_2 \approx -13\Gamma_L$  with topological regions still being present.

### III. QUANTUM GEOMETRY AND MICROWAVE SPECTROSCOPY

The quantum geometry of each ABS  $|\psi_n\rangle$  is described by the quantum geometric tensor (QGT) [74]

$$q_{\alpha\beta}^{(n)} = \langle \partial_{\alpha} \psi_n | (1 - |\psi_n\rangle \langle \psi_n|) | \partial_{\beta} \psi_n \rangle = \sum_{\substack{m=-N \\ m \neq 0, n}}^N q_{\alpha\beta}^{(nm)}, \quad (6)$$

with the elements  $q_{\alpha\beta}^{(nm)} = \langle \partial_{\alpha} \psi_n | \psi_m \rangle \langle \psi_m | \partial_{\beta} \psi_n \rangle$  and again  $\partial_{\alpha} \equiv \partial / \partial \varphi_{\alpha}$ . Furthermore, we obtain the (Fubini-Study) metric tensor  $g_{\alpha\beta}^{(n)} = \text{Re}(q_{\alpha\beta}^{(n)})$  and the Berry curvature  $f_{\alpha\beta}^{(n)} = -2 \text{Im}(q_{\alpha\beta}^{(n)})$  from the real and imaginary part of the QGT, respectively.

In the following, we aim at applying the method of microwave spectroscopy described in Ref. [32] in the presence of more than one nondegenerate pair of ABS. In general, Eq. (6) implies a priori that we need to measure all possible nonadiabatic transitions between a certain state  $|\psi_n\rangle$  and all the other states  $|\psi_m\rangle$  ( $n \neq m$ ) by microwave spectroscopy to construct the QGT of this particular single-particle state  $|\psi_n\rangle$ , as sketched in Fig. 3. We will first describe the general procedure and later discuss possible experimental difficulties.

On the one hand, in order to measure the diagonal elements  $q_{\alpha\alpha}^{(nm)}$  of the QGT, we need to apply a small perturbation ( $A/\hbar\omega \ll 1$ ) to one phase  $\varphi_{\alpha} \rightarrow \varphi_{\alpha} + 2A \cos(\omega t)/\hbar\omega$ , resulting in the transition (photon absorption) with a rate  $R_{n \rightarrow m, \alpha\alpha} = r_{n \rightarrow m, \alpha\alpha} \delta(\varepsilon_m - \varepsilon_n - \hbar\omega)$  with the oscillator strength [32, 75]

$$r_{n \rightarrow m, \alpha\alpha} = \frac{2\pi}{\hbar} A^2 q_{\alpha\alpha}^{(nm)} \quad (7)$$

according to Fermi's golden rule. On the other hand, we assume to simultaneously apply two small perturbations,  $\varphi_{\alpha} \rightarrow \varphi_{\alpha} + 2A \cos(\omega t)/\hbar\omega$  to one phase and  $\varphi_{\beta} \rightarrow \varphi_{\beta} + 2A \cos(\omega t - \gamma)/\hbar\omega$  to another phase ( $\alpha \neq \beta$ ) with a fixed phase difference  $\gamma$  between the two modulations, to measure the off-diagonal elements  $q_{\alpha\beta}^{(nm)}$  of the QGT. The resulting transition rates are  $R_{n \rightarrow m, \alpha\beta}^{(\gamma)} =$



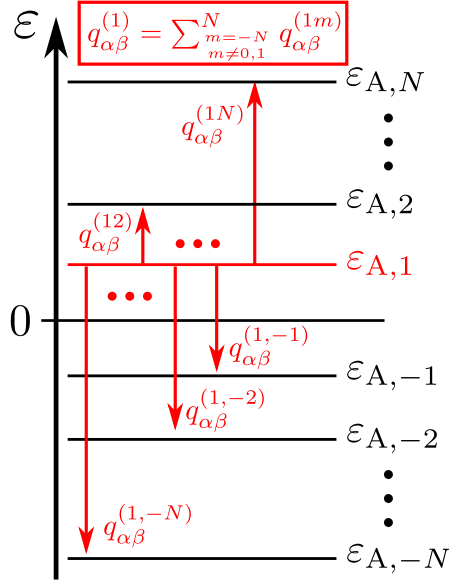


FIG. 3. Different contributions of the elements  $q_{\alpha\beta}^{(1m)}$  from other ABS with energies  $\epsilon_{A,m}$  ( $m \neq 0, 1$ ) to the QGT  $q_{\alpha\beta}^{(1)}$  of the ABS with energy  $\epsilon_{A,1}$  according to Eq. (6).

$r_{n \rightarrow m, \alpha\beta}^{(\gamma)} \delta(\epsilon_m - \epsilon_n - \hbar\omega)$  with the oscillator strength [32, 75]

$$r_{n \rightarrow m, \alpha\beta}^{(\gamma)} = \frac{2\pi A^2}{\hbar} \left\{ q_{\alpha\alpha}^{(nm)} + q_{\beta\beta}^{(nm)} + e^{i\gamma} q_{\alpha\beta}^{(nm)} + e^{-i\gamma} q_{\beta\alpha}^{(nm)} \right\}, \quad (8)$$

which now depends on the relative phase difference  $\gamma$  between the two drives. Details of the derivation of Eqs. (7) and (8) are presented in Appendix C. By comparing Eqs. (7) and (8) with the definition of the QGT in Eq. (6), we obtain the relations

$$g_{\alpha\alpha}^{(n)} = \frac{\hbar}{2\pi A^2} \sum_{\substack{m=-N \\ m \neq 0, n}}^N r_{n \rightarrow m, \alpha\alpha}, \quad (9a)$$

$$g_{\alpha\beta}^{(n)} = \frac{\hbar}{8\pi A^2} \sum_{\substack{m=-N \\ m \neq 0, n}}^N [r_{n \rightarrow m, \alpha\beta}^{(0)} - r_{n \rightarrow m, \alpha\beta}^{(\pi)}], \quad (9b)$$

$$f_{\alpha\beta}^{(n)} = \frac{\hbar}{4\pi A^2} \sum_{\substack{m=-N \\ m \neq 0, n}}^N [r_{n \rightarrow m, \alpha\beta}^{(\pi/2)} - r_{n \rightarrow m, \alpha\beta}^{(-\pi/2)}]. \quad (9c)$$

This allows us to measure the metric tensor by linear microwave spectroscopy, i.e., modulating one phase or two phases with  $\gamma = 0, \pi$ , while the Berry curvature follows from circular microwave spectroscopy, i.e., modulating two phases with  $\gamma = \pm\pi/2$ .

Although this seems to be straightforward to implement, the experimental difficulty at very low temperature is to measure the transitions between two occupied

or two empty states, respectively. To overcome this obstacle, one could either perform the experiment at sufficiently high temperatures, for which previously filled (empty) states get partially depopulated (populated), or one could use pulses to empty/fill a certain state before measuring the transition.

Fortunately, for low-temperature quantum transport, the experimentally relevant quantity is the QGT of the many-body GS which, in the noninteracting case, can be constructed from the elements in Eq. (9), as shown in Appendix C. The resulting many-body Berry curvature and metric tensor of the GS,  $F_{\alpha\beta}^{(\text{GS})}$  and  $G_{\alpha\beta}^{(\text{GS})}$ , respectively, are still accessible via microwave spectroscopy even at zero temperature and the result simply reads

$$G_{\alpha\alpha}^{(\text{GS})} = \frac{\hbar}{2\pi A^2} \sum_{j \in D^-} \sum_{k \in D^+} r_{j \rightarrow k, \alpha\alpha}, \quad (10a)$$

$$G_{\alpha\beta}^{(\text{GS})} = \frac{\hbar}{8\pi A^2} \sum_{j \in D^-} \sum_{k \in D^+} (r_{j \rightarrow k, \alpha\beta}^{(0)} - r_{j \rightarrow k, \alpha\beta}^{(\pi)}), \quad (10b)$$

$$F_{\alpha\beta}^{(\text{GS})} = \frac{\hbar}{4\pi A^2} \sum_{j \in D^-} \sum_{k \in D^+} (r_{j \rightarrow k, \alpha\beta}^{(\pi/2)} - r_{j \rightarrow k, \alpha\beta}^{(-\pi/2)}), \quad (10c)$$

which shows that, indeed, only transitions from occupied ( $D^-$ ) to empty states ( $D^+$ ) are needed. Both the GS Berry curvature and the GS metric tensor can therefore be simply obtained from all the experimentally accessible transitions by using microwave spectroscopy. In Fig. 4, we show, as an example of Eq. (10), the metric tensor and the Berry curvature of the GS for  $N = 3$  dots in the topological region for  $\varphi_3 = 0.4\pi$  in which we find a Chern number  $C_{12}^{(\text{GS})} = -1$  [cf. Fig. 2(c)]. A local measurement of the elements of the QGT by microwave spectroscopy will not only reveal the topological phase in terms of the Chern number by integrating the Berry curvature, it is also possible to locate Weyl points in phase space  $\mathbb{T}^N$  for which zero-energy states are expected. In fact, Fig. 4 shows that there are regions where the elements of the QGT are significantly different from zero, signaling the location of a Weyl point. In fact, the Weyl point is located at  $\varphi_W/\pi \approx (1.603, 0.781, 0.384)$ , with the  $\varphi_1$  and  $\varphi_2$  coordinates indicated in the plots. While possible zero-energy states might be useful on its own, let us recall here that the Chern number will be responsible for a quantized transconductance across two terminals [22].

#### IV. DISCUSSION AND CONCLUSION

In this work we have proposed an experimentally feasible system consisting of a linear chain of  $N$  quantum dots connected to  $N + 1$  s-wave superconducting leads, as shown in Fig. 1. This linear setup does not require a direct connection between the different superconducting terminals, as opposed to the system considered in Ref. [32], which might take a lot of engineering effort to realize in practice. We have derived an effective low-energy Hamiltonian of the chain, presented in Eq. (1),

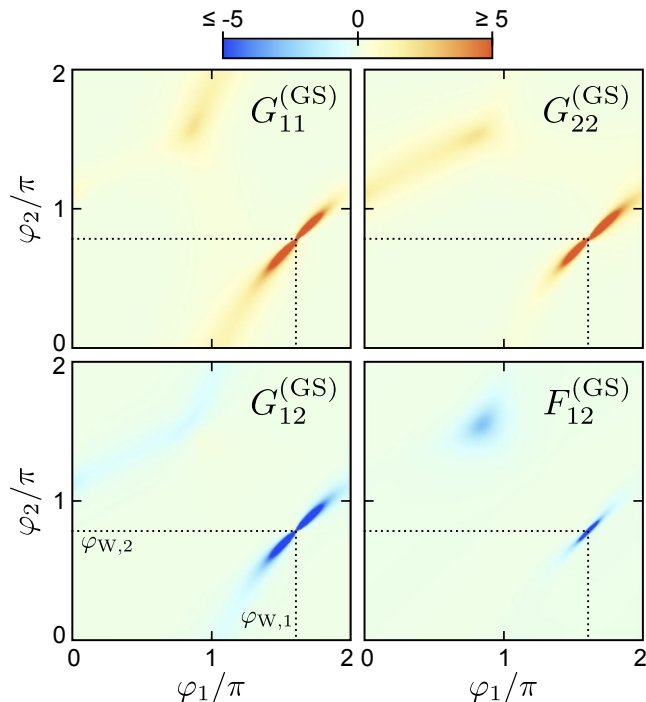


FIG. 4. Ground state metric tensor  $G_{12}^{(\text{GS})}$  and Berry curvature  $F_{12}^{(\text{GS})}$  for  $N = 3$  dots at  $\varphi_3 = 0.4\pi$  in the topological phase with  $C_{12}^{(\text{GS})} = -1$  [cf. Fig. 2(c)]. The elements of the QGT are strongly peaked for values of  $\varphi$  close to a Weyl point. The coordinates of the Weyl point indicated in this plot are  $\varphi^{\text{W}} = (\varphi_{\text{W},1}, \varphi_{\text{W},2}, \varphi_{\text{W},3}) \approx (1.603, 0.781, 0.384)\pi$  [cf. lower red dot in Fig. 2(b)]. The visible range of values of the elements of the QGT has been limited from  $-5$  to  $+5$  to make the overall structure for small values visible. In fact, the values of the elements of the QGT at the point  $(\varphi_{\text{W},1}, \varphi_{\text{W},2})$  are exceeding  $\pm 800$ . Parameters:  $\Gamma_{\text{NL}} = 0.8\Gamma_{\text{L}}$ ,  $w = 0.2\Gamma_{\text{L}}$ ,  $\varepsilon_1 = -\varepsilon_2 = \varepsilon_3 = -\Gamma_{\text{L}}/2$ ,  $\varphi_0 = 0$ .

which reveals large topological regions in terms of the integer-valued Chern number and, therefore, leaves large experimental freedom for the concrete values of the various system parameters to study quantum geometry and topology in the synthetic space of  $N$  independent superconducting phases [cf. Fig. 2]. In particular, as discussed in Fig. 2(c), it is also not necessary for the dots to be directly coupled ( $w = 0$ ) and it turns out that a larger value of the direct coupling can even lead to an enhancement of the robustness of the topological phase ( $w = 2\Gamma_{\text{L}}$ ). We furthermore believe that this or similar engineered systems also provide useful and easily scalable condensed-matter realizations to study higher-dimensional topological invariants such as, e.g., higher-dimensional Chern numbers [76–87] or the so-called Dixmier-Douady invariants [88–92], since the synthetic dimension  $N$  of the space of superconducting phases  $\mathbb{T}^N$  scales with the number of superconducting leads which can be, in principle, arbitrary.

Moreover, we have worked out the insightful connection between the QGT of single-particle ABS and the

QGT of the corresponding noninteracting many-body GS. At this point we want to stress that this connection is relevant to any physical system hosting multiple energy bands. As only the geometrical property of the GS is of particular importance for low-temperature experiments, we have shown that, although the QGT of an individual ABS cannot be accessed without further preparation, the QGT of the GS as a whole as presented in Eq. (10) is still accessible by microwave spectroscopy from the oscillator strengths of multiple absorption lines. In this regard, we have generalized the previously discussed application of microwave spectroscopy to measure the QGT of topological Josephson matter in Ref. [32] to the case of the presence of multiple ABS. We emphasize that this method provides an alternative way to measure the GS topology beyond the already mentioned transconductance measurements originally proposed in Ref. [22]. Furthermore, microwave spectroscopy provides a tool to gain access to the local QGT and makes it possible to localize the position of zero-energy states through the measurement of Weyl points in phase space [cf. Fig. 4].

Since it is based on quantum dots, our system provides an ideal starting point to study the effect of Coulomb interactions on the geometry and topology of the GS. Furthermore, it may be relevant for concrete experiments to study the effect of a finite superconducting gap, which can be of the order of the tunneling [66, 67], and the influence of the continuum [28, 93] on the quantum geometry of the GS, which is not captured in our low-energy theory at infinite gap. Finally, the general role of a finite temperature and dissipation on both quantum geometry and topology remains an open question, both theoretically and experimentally [94–96], and it will be interesting to apply these concepts to the proposed system in the future.

## ACKNOWLEDGMENTS

We thank Hannes Weisbrich, Hugues Pothier, and Cristian Urbina for useful discussions. This work was supported by the Deutsche Forschungsgemeinschaft through SFB 767 and Grant No. RA 2810/1. J.C.C. acknowledges the support via the Mercator Program of the DFG in the frame of the SFB 767.

### Appendix A: Effective Hamiltonian for $N$ dots

Here, we derive the effective Hamiltonian of  $N$  dots connected to  $N+1$  superconducting terminals as sketched in Fig. 1. Due to the inclusion of superconductivity, we start by defining a set of Pauli matrices  $(\tau_1, \tau_2, \tau_3)$  in Nambu space. The starting Hamiltonian reads

$$H = H_{\text{D}} + H_{\text{S}} + H_{\text{DS}}. \quad (\text{A1})$$

The  $N$  dots and their couplings are described by  $H_{\text{D}} = \mathbf{d}^\dagger \hat{H}_{\text{D}} \mathbf{d}$ , where the  $2N \times 2N$  matrix Hamiltonian is given

by

$$\hat{H}_D = \begin{pmatrix} \varepsilon_1 & w_{12} & 0 & \cdots & 0 & 0 \\ w_{12} & \varepsilon_2 & w_{23} & \cdots & 0 & 0 \\ 0 & w_{23} & \varepsilon_3 & \cdots & 0 & 0 \\ \vdots & \vdots & \vdots & \ddots & \vdots & \vdots \\ 0 & 0 & 0 & \cdots & \varepsilon_{N-1} & w_{N-1,N} \\ 0 & 0 & 0 & \cdots & w_{N-1,N} & \varepsilon_N \end{pmatrix} \otimes \tau_3 \quad (\text{A2})$$

with  $\varepsilon_j$  being the onsite energy of dot  $j$ ,  $w_{j,j+1}$  being the hopping energy between dots  $j$  and  $j+1$ , and  $\mathbf{d}^\dagger = (d_{1\uparrow}^\dagger, d_{1\downarrow}^\dagger, d_{2\uparrow}^\dagger, d_{2\downarrow}^\dagger, \dots, d_{N\uparrow}^\dagger, d_{N\downarrow}^\dagger)$  is the Nambu spinor consisting of electronic annihilation (creation) operators  $d_{j\sigma}^{(\dagger)}$  of spin  $\sigma = \uparrow, \downarrow$  on dot  $j$ .

The Hamiltonian describing the  $N+1$  BCS superconducting leads reads  $H_S = \sum_{\mathbf{k}} \mathbf{c}_{\mathbf{k}}^\dagger \hat{H}_{S,\mathbf{k}} \mathbf{c}_{\mathbf{k}}$ , with  $\mathbf{c}_{\mathbf{k}}^\dagger = (c_{0\mathbf{k}\uparrow}^\dagger, c_{0(-\mathbf{k})\downarrow}^\dagger, c_{1\mathbf{k}\uparrow}^\dagger, c_{1(-\mathbf{k})\downarrow}^\dagger, \dots, c_{N\mathbf{k}\uparrow}^\dagger, c_{N(-\mathbf{k})\downarrow}^\dagger)$  containing electronic annihilation (creation) operators  $c_{j\mathbf{k}\sigma}^{(\dagger)}$  of quasimomentum  $\mathbf{k}$  and spin  $\sigma$  in lead  $j$ , and the  $2(N+1) \times 2(N+1)$  diagonal matrix Hamiltonian

$$\hat{H}_{S,\mathbf{k}} = \text{diag}(\hat{H}_{S,0\mathbf{k}}, \hat{H}_{S,1\mathbf{k}}, \dots, \hat{H}_{S,N\mathbf{k}}). \quad (\text{A3})$$

Here,  $\hat{H}_{S,j\mathbf{k}} = \xi_{j\mathbf{k}}\tau_3 + \Delta_j e^{i\varphi_j\tau_3}\tau_1$ , where  $\Delta_j$  and  $\varphi_j$  are the superconducting pairing potential and phase, respectively, and  $\xi_{j\mathbf{k}}$  is the normal state dispersion in each lead.

Finally, the coupling between the dots and neighboring superconducting leads is given by

$$H_{DS} = \sum_{\mathbf{k}} (\mathbf{d}^\dagger \hat{V}_{DS} \mathbf{c}_{\mathbf{k}} + \text{h.c.}), \quad (\text{A4})$$

with the  $2N \times 2(N+1)$  matrix coupling

$$\hat{V}_{DS} = \begin{pmatrix} t_{10} & t_{11} & 0 & 0 & \cdots & 0 & 0 \\ 0 & t_{21} & t_{22} & 0 & \cdots & 0 & 0 \\ 0 & 0 & t_{32} & t_{33} & \cdots & 0 & 0 \\ \vdots & \vdots & \vdots & \vdots & \ddots & \vdots & \vdots \\ 0 & 0 & 0 & 0 & \cdots & t_{N,N-1} & t_{NN} \end{pmatrix} \otimes \tau_3 \quad (\text{A5})$$

and the hopping energy  $t_{jk}$  between dot  $j$  and lead  $k$ .

We use the Green's function (GF) technique to derive an effective Hamiltonian of the subsystem of the dots. From  $\hat{g}_{S,j\mathbf{k}} = (\varepsilon - \hat{H}_{S,j\mathbf{k}})^{-1}$ , we find the  $2 \times 2$  GF of the  $j$ -th lead as

$$\hat{g}_{S,j\mathbf{k}} = \frac{\varepsilon - \xi_{j\mathbf{k}} + \Delta_j e^{i\varphi_j\tau_3}\tau_1}{\varepsilon^2 - \xi_{j\mathbf{k}}^2 - \Delta_j^2}. \quad (\text{A6})$$

Since the dots and hoppings do not depend on quasimomentum  $\mathbf{k}$ , we sum over all quasimomenta and define  $\hat{g}_{S,j} = \sum_{\mathbf{k}} \hat{g}_{S,j\mathbf{k}}$ . Turning the summation into an energy integration in the wide-band limit via  $\sum_{\mathbf{k}} \rightarrow N_0 \int d\xi_{j\mathbf{k}}$ , with  $N_0$  being the normal state density of states at the Fermi energy, we obtain

$$\hat{g}_{S,j} = -\pi N_0 \frac{\varepsilon + \Delta_j e^{i\varphi_j\tau_3}\tau_1}{\sqrt{\Delta_j^2 - \varepsilon^2}} \xrightarrow{\Delta_j \rightarrow \infty} -\pi N_0 e^{i\varphi_j\tau_3}\tau_1, \quad (\text{A7})$$

where we assume that the pairing potentials are larger than all relevant energy scales. Finally, the bare  $2(N+1) \times 2(N+1)$  matrix GF of the subsystem of the superconducting leads is given by the diagonal matrix

$$\hat{g}_S = \text{diag}(\hat{g}_{S,0}, \dots, \hat{g}_{S,N}), \quad (\text{A8})$$

written in the basis  $\mathbf{c}^\dagger = (\mathbf{c}_0^\dagger, \dots, \mathbf{c}_N^\dagger) = \sum_{\mathbf{k}} \mathbf{c}_{\mathbf{k}}^\dagger$ .

Formally, the bare  $2N \times 2N$  matrix GF of the dots with their couplings is given by  $\hat{g}_D = (\varepsilon - \hat{H}_D)^{-1}$ . The explicit form of  $\hat{g}_D$  is not needed for the following derivation.

We define an effective matrix Hamiltonian  $\hat{H}_{\text{eff}}^{(N)}$  from the dressed GF of the  $2N \times 2N$  dot subsystem, i.e.,  $\hat{G}_D = (\varepsilon - \hat{H}_{\text{eff}}^{(N)})^{-1}$ , which is the solution of the Dyson equation  $\hat{G}_D = \hat{g}_D + \hat{g}_D \hat{\Sigma}_D \hat{G}_D$ , with the self-energy  $\hat{\Sigma}_D = \hat{V}_{DS} \hat{g}_S \hat{V}_{DS}^\dagger$ . Using the formal definition of  $\hat{g}_D$ , we obtain the solution  $\hat{H}_{\text{eff}}^{(N)} = \hat{H}_D + \hat{\Sigma}_D$  which describes the dots proximity coupled to the superconductors. Finally, the effective low-energy Hamiltonian is

$$H_{\text{eff}} = \mathbf{d}^\dagger \hat{H}_{\text{eff}}^{(N)} \mathbf{d} = H_D + H_{\text{LP}} + H_{\text{NLP}}, \quad (\text{A9})$$

with the local and nonlocal pairings (LP and NLP) originating from the self-energy  $\hat{\Sigma}_D$  given by

$$H_{\text{LP}} = \sum_{j=1}^N \mathbf{d}_j^\dagger (\Gamma_j^{(j-1)} e^{i\varphi_{j-1}\tau_3} + \Gamma_{jj}^{(j)} e^{i\varphi_j\tau_3}) \tau_1 \mathbf{d}_j, \quad (\text{A10a})$$

$$H_{\text{NLP}} = \sum_{j=1}^{N-1} \Gamma_{j,j+1}^{(j)} (\mathbf{d}_j^\dagger e^{i\varphi_j\tau_3} \tau_1 \mathbf{d}_{j+1} + \mathbf{d}_{j+1}^\dagger e^{i\varphi_{j+1}\tau_3} \tau_1 \mathbf{d}_j), \quad (\text{A10b})$$

with  $\Gamma_j^{(k)} = \pi N_0 t_{jk}^2$ ,  $\Gamma_{j,j+1}^{(k)} = \pi N_0 t_{jk} t_{j+1,k}$  and the local Nambu spinors  $\mathbf{d}_j^\dagger = (d_{j\uparrow}^\dagger, d_{j\downarrow}^\dagger)$ . Eq. (A9), together with Eq. (A10), represents the effective Hamiltonian presented in Eq. (1) in Sec. II of the main text.

## Appendix B: Quantum geometry of general fermionic $n$ -particle many-body states

For  $n \in \mathbb{N}$ , let  $|\psi_j\rangle$ ,  $j \in \{1, \dots, n\}$ , be single-particle states with their individual single-particle quantum geometric tensors (QGTs)

$$q_{\alpha\beta}^{(j)} = \langle \partial_\alpha \psi_j | (1 - |\psi_j\rangle \langle \psi_j|) | \partial_\beta \psi_j \rangle, \quad (\text{B1})$$

their Berry curvatures  $f_{\alpha\beta}^{(j)} = -2 \text{Im}(q_{\alpha\beta}^{(j)})$  and their (Fubini-Study) metric tensors  $g_{\alpha\beta}^{(j)} = \text{Re}(q_{\alpha\beta}^{(j)})$ . The different single-particle states shall be orthonormalized, i.e.,  $\langle \psi_j | \psi_k \rangle = \delta_{jk}$ . Furthermore, let

$$|\Psi_n\rangle = \frac{1}{\sqrt{n!}} \sum_{\mathcal{P}} (-1)^P \mathcal{P} [|\psi_1\rangle \otimes \cdots \otimes |\psi_n\rangle] \quad (\text{B2})$$

be the corresponding general antisymmetric many-body fermionic state, in which we sum over all  $n!$  different permutations with the permutation operator  $\mathcal{P}$  and the number of transpositions  $p$  of a particular permutation. How are the single-particle QGTs related to the corresponding many-body QGT

$$Q_{\alpha\beta}^{(n)} = \langle \partial_\alpha \Psi_n | (1 - |\Psi_n\rangle \langle \Psi_n|) | \partial_\beta \Psi_n \rangle \quad (\text{B3})$$

and, in particular, what are the corresponding relations to the many-body Berry curvature  $F_{\alpha\beta}^{(n)} = -2 \text{Im}(Q_{\alpha\beta}^{(n)})$  and the metric tensor  $G_{\alpha\beta}^{(n)} = \text{Re}(Q_{\alpha\beta}^{(n)})$  of the  $n$ -particle state  $|\Psi_n\rangle$ ?

After a lengthy but straightforward calculation, the final result reads

$$G_{\alpha\beta}^{(n)} = \sum_{j=1}^n g_{\alpha\beta}^{(j)} - \sum_{\substack{j,k=1 \\ j \neq k}}^n \langle \partial_\alpha \psi_j | \psi_k \rangle \langle \psi_k | \partial_\beta \psi_j \rangle, \quad (\text{B4a})$$

$$F_{\alpha\beta}^{(n)} = \sum_{j=1}^n f_{\alpha\beta}^{(j)}. \quad (\text{B4b})$$

While the result for the metric tensor reveals a nontrivial and less intuitive relation, the result for the Berry curvature can be understood more intuitively and matches the expected result. On an intuitive level, suppose that the single-particle states acquire the Berry phases  $\phi_j$  according to  $|\psi_j\rangle \mapsto e^{i\phi_j} |\psi_j\rangle$  after a cyclic evolution in parameter space [71]. Then, the evolution of the corresponding many-body state results in

$$|\Psi_n\rangle \mapsto e^{i\Phi_n} |\Psi_n\rangle \quad (\text{B5})$$

according to the definition in Eq. (B2), where the Berry phase  $\Phi_n = \sum_{j=1}^n \phi_j$  is the sum of the individual Berry phases  $\phi_j$ . This directly translates to the Berry curvature by means of Stokes' integral theorem.

As a direct consequence of Eq. (B4b), the Chern number of the many-body GS is simply given by the sum of all individual Chern numbers of the occupied single-particle states as expected, i.e.,

$$C_{\alpha\beta}^{(\text{GS})} = \sum_{j=1}^n c_{\alpha\beta}^{(j)}, \quad (\text{B6})$$

which is also the result presented in Eq. (5) in Sec. II of the main text.

### Appendix C: Microwave spectroscopy of the quantum geometry of the many-body ground state

For the diagonal elements,  $q_{\alpha\alpha}^{(n)} = g_{\alpha\alpha}^{(n)}$ , we need to apply a perturbation to one phase  $\varphi_\alpha \rightarrow \varphi_\alpha + 2A \cos(\omega t)/\hbar\omega$ , resulting the transition rate  $R_{n \rightarrow m, \alpha\alpha} = r_{n \rightarrow m, \alpha\alpha} \delta(\varepsilon_m - \varepsilon_n - \hbar\omega)$  with the oscillator strength [32, 75]

$$r_{n \rightarrow m, \alpha\alpha} = \frac{2\pi A^2 |\langle \psi_m | (\partial_\alpha \hat{H}_{\text{eff}}^{(N)}) | \psi_n \rangle|^2}{\hbar(\varepsilon_m - \varepsilon_n)^2} \quad (\text{C1})$$

according to Fermi's golden rule. In order to measure the off-diagonal elements of the QGT  $q_{\alpha\beta}^{(n)}$  for  $\alpha \neq \beta$ , we need to simultaneously apply the perturbations  $\varphi_\alpha \rightarrow \varphi_\alpha + 2A \cos(\omega t)/\hbar\omega$  and  $\varphi_\beta \rightarrow \varphi_\beta + 2A \cos(\omega t - \gamma)/\hbar\omega$  with a phase difference  $\gamma$ , resulting in the transition rates  $R_{n \rightarrow m, \alpha\beta}^{(\gamma)} = r_{n \rightarrow m, \alpha\beta}^{(\gamma)} \delta(\varepsilon_m - \varepsilon_n - \hbar\omega)$  with the oscillator strength [32, 75]

$$r_{n \rightarrow m, \alpha\beta}^{(\gamma)} = \frac{2\pi A^2 |\langle \psi_m | (\partial_\alpha \hat{H}_{\text{eff}}^{(N)} + e^{i\gamma} \partial_\beta \hat{H}_{\text{eff}}^{(N)}) | \psi_n \rangle|^2}{\hbar(\varepsilon_m - \varepsilon_n)^2} \quad (\text{C2})$$

according to Fermi's golden rule. Notice that  $r_{n \rightarrow m, \alpha\beta}^{(\gamma)} = r_{m \rightarrow n, \alpha\beta}^{(-\gamma)}$  by definition. Using the identities

$$\langle \partial_\alpha \psi_n | \psi_m \rangle = -\langle \psi_n | \partial_\alpha \psi_m \rangle, \quad (\text{C3a})$$

$$\langle \psi_n | (\partial_\alpha \hat{H}_{\text{eff}}^{(N)}) | \psi_m \rangle = (\varepsilon_n - \varepsilon_m) \langle \partial_\alpha \psi_n | \psi_m \rangle, \quad (\text{C3b})$$

for  $n \neq m$ , we obtain

$$r_{n \rightarrow m, \alpha\alpha} = \frac{2\pi A^2}{\hbar} q_{\alpha\alpha}^{(nm)}, \quad (\text{C4a})$$

$$r_{n \rightarrow m, \alpha\beta}^{(\gamma)} = \frac{2\pi A^2}{\hbar} \left\{ q_{\alpha\alpha}^{(nm)} + q_{\beta\beta}^{(nm)} + e^{i\gamma} q_{\alpha\beta}^{(nm)} + e^{-i\gamma} q_{\beta\alpha}^{(nm)} \right\}. \quad (\text{C4b})$$

which are exactly Eqs. (7) and (8) as presented in Sec. III of the main text. Finally, for  $\alpha \neq \beta$ , this yields the useful identities

$$\text{Re}(q_{\alpha\beta}^{(nm)}) = \frac{\hbar}{8\pi A^2} (r_{n \rightarrow m, \alpha\beta}^{(0)} - r_{n \rightarrow m, \alpha\beta}^{(\pi)}), \quad (\text{C5a})$$

$$\text{Im}(q_{\alpha\beta}^{(nm)}) = -\frac{\hbar}{8\pi A^2} (r_{n \rightarrow m, \alpha\beta}^{(\pi/2)} - r_{n \rightarrow m, \alpha\beta}^{(-\pi/2)}). \quad (\text{C5b})$$

At zero temperature, the many-body ground state is given by an (antisymmetric) combination of all  $N$  occupied single-particle states up to the Fermi energy, as generally defined in Eq. (B2). We now use the general result in Eq. (B4) to relate the measured oscillator strengths from microwave spectroscopy to the Berry curvature  $F_{\alpha\beta}^{(\text{GS})}$  and the metric tensor  $G_{\alpha\beta}^{(\text{GS})}$  of the ground state.



For the Berry curvature, we obtain

$$\begin{aligned}
F_{\alpha\beta}^{(\text{GS})} &\stackrel{\text{(B4b)}}{=} \sum_{j=-N}^{-1} f_{\alpha\beta}^{(j)} \stackrel{\text{(6)}}{=} -2 \sum_{j=-N}^{-1} \sum_{\substack{k=-N \\ k \neq 0, j}}^N \text{Im}(q_{\alpha\beta}^{(jk)}) \\
&\stackrel{\text{(C5b)}}{=} \frac{\hbar}{4\pi A^2} \sum_{j=-N}^{-1} \sum_{\substack{k=-N \\ k \neq 0, j}}^N (r_{j \rightarrow k, \alpha\beta}^{(\pi/2)} - r_{j \rightarrow k, \alpha\beta}^{(-\pi/2)}) \\
&= \frac{\hbar}{4\pi A^2} \left[ \underbrace{\sum_{\substack{j, k=-N \\ k \neq j}}^{-1} (r_{j \rightarrow k, \alpha\beta}^{(\pi/2)} - r_{j \rightarrow k, \alpha\beta}^{(-\pi/2)})}_{=0, \text{ Eq. (C2)}} \right. \\
&\quad \left. + \sum_{j=-N}^{-1} \sum_{k=1}^N (r_{j \rightarrow k, \alpha\beta}^{(\pi/2)} - r_{j \rightarrow k, \alpha\beta}^{(-\pi/2)}) \right] \\
&= \frac{\hbar}{4\pi A^2} \sum_{j=-N}^{-1} \sum_{k=1}^N (r_{j \rightarrow k, \alpha\beta}^{(\pi/2)} - r_{j \rightarrow k, \alpha\beta}^{(-\pi/2)}), \quad (\text{C6})
\end{aligned}$$

which is the one presented in Eq. (10c) in Sec. III of the main text.

For the metric tensor, we obtain

$$\begin{aligned}
G_{\alpha\beta}^{(\text{GS})} &\stackrel{\text{(B4a)}}{=} \sum_{j=-N}^{-1} g_{\alpha\beta}^{(j)} - \sum_{\substack{j, k=-N \\ j \neq k}}^{-1} \langle \partial_\alpha \psi_j | \psi_k \rangle \langle \psi_k | \partial_\beta \psi_j \rangle \\
&\stackrel{\text{(6)}}{=} \sum_{j=-N}^{-1} \sum_{\substack{k=-N \\ k \neq 0, j}}^N \text{Re}(q_{\alpha\beta}^{(jk)}) - \sum_{\substack{j, k=-N \\ k \neq j}}^{-1} q_{\alpha\beta}^{(jk)} \\
&= \sum_{j=-N}^{-1} \sum_{\substack{k=-N \\ k \neq 0, j}}^N \text{Re}(q_{\alpha\beta}^{(jk)}) - \frac{1}{2} \sum_{\substack{j, k=-N \\ k \neq j}}^{-1} \underbrace{(q_{\alpha\beta}^{(jk)} + q_{\alpha\beta}^{(kj)})}_{2 \text{Re}(q_{\alpha\beta}^{(jk)})} \\
&= \sum_{j=-N}^{-1} \sum_{k=1}^N \text{Re}(q_{\alpha\beta}^{(jk)}). \quad (\text{C7})
\end{aligned}$$

In both cases we see that we only need to measure transitions between occupied and empty states. Finally, we get for the diagonal and off-diagonal elements

$$G_{\alpha\alpha}^{(\text{GS})} \stackrel{\text{(C4a)}}{=} \frac{\hbar}{2\pi A^2} \sum_{j=-N}^{-1} \sum_{k=1}^N r_{j \rightarrow k, \alpha\alpha}, \quad (\text{C8a})$$

$$G_{\alpha\beta}^{(\text{GS})} \stackrel{\text{(C5a)}}{=} \frac{\hbar}{8\pi A^2} \sum_{j=-N}^{-1} \sum_{k=1}^N (r_{j \rightarrow k, \alpha\beta}^{(0)} - r_{j \rightarrow k, \alpha\beta}^{(\pi)}), \quad (\text{C8b})$$

which are the relations presented in Eqs. (10a) and (10b), respectively, in Sec. III of the main text.

- 
- [1] A. Bansil, H. Lin, and T. Das, Colloquium: Topological band theory, *Rev. Mod. Phys.* **88**, 021004 (2016).
- [2] C. L. Kane and E. J. Mele,  $Z_2$  Topological Order and the Quantum Spin Hall Effect, *Phys. Rev. Lett.* **95**, 146802 (2005).
- [3] M. Z. Hasan and C. L. Kane, Colloquium: Topological insulators, *Rev. Mod. Phys.* **82**, 3045 (2010).
- [4] N. P. Armitage, E. J. Mele, and A. Vishwanath, Weyl and Dirac semimetals in three-dimensional solids, *Rev. Mod. Phys.* **90**, 015001 (2018).
- [5] M. Sato and Y. Ando, Topological superconductors: A review, *Rep. Prog. Phys.* **80**, 076501 (2017).
- [6] K. Kawabata, K. Shiozaki, M. Ueda, and M. Sato, Symmetry and Topology in Non-Hermitian Physics, *Phys. Rev. X* **9**, 041015 (2019).
- [7] A. Y. Kitaev, Unpaired Majorana fermions in quantum wires, *Phys. Usp.* **44**, 131 (2001).
- [8] A. Y. Kitaev, Fault-tolerant quantum computation by anyons, *Annals of Physics* **303**, 2–30 (2003).
- [9] L. Fu and C. L. Kane, Superconducting Proximity Effect and Majorana Fermions at the Surface of a Topological Insulator, *Phys. Rev. Lett.* **100**, 096407 (2008).
- [10] G. Yang, Z. Lyu, J. Wang, J. Ying, X. Zhang, J. Shen, G. Liu, J. Fan, Z. Ji, X. Jing, F. Qu, and L. Lu, Protected gap closing in Josephson trijunctions constructed on  $\text{Bi}_2\text{Te}_3$ , *Phys. Rev. B* **100**, 180501(R) (2019).
- [11] N. M. Chtchelkatchev and Y. V. Nazarov, Andreev Quantum Dots for Spin Manipulation, *Phys. Rev. Lett.* **90**, 226806 (2003).
- [12] A. Zazunov, V. S. Shumeiko, E. N. Bratus, J. Lantz, and G. Wendin, Andreev Level Qubit, *Phys. Rev. Lett.* **90**, 087003 (2003).
- [13] L. Bretheau, Ç. Ö. Girit, H. Pothier, D. Esteve, and C. Urbina, Exciting Andreev pairs in a superconducting atomic contact, *Nature (London)* **499**, 312 (2013).
- [14] C. Janvier, L. Tosi, L. Bretheau, Ç. Ö. Girit, M. Stern, P. Bertet, P. Joyez, D. Vion, D. Esteve, M. F. Goffman, H. Pothier, and C. Urbina, Coherent manipulation of Andreev states in superconducting atomic contacts, *Science* **349**, 1199 (2015).
- [15] D. J. van Woerkom, A. Proutski, B. van Heck, D. Bouman, J. I. Väyrynen, L. I. Glazman, P. Krogstrup, J. Nygård, L. P. Kouwenhoven, and A. Geresdi, Microwave spectroscopy of spinful Andreev bound states in ballistic semiconductor Josephson junctions, *Nat. Phys.* **13**, 876 (2017).
- [16] M. Hays, G. de Lange, K. Serniak, D. J. van Woerkom, D. Bouman, P. Krogstrup, J. Nygård, A. Geresdi, and M. H. Devoret, Direct Microwave Measurement of Andreev-Bound-State Dynamics in a Semiconductor-Nanowire Josephson Junction, *Phys. Rev. Lett.* **121**, 047001 (2018).
- [17] J.-D. Pillet, C. H. L. Quay, P. Morfin, C. Bena, A. Levy Yeyati, and P. Joyez, Andreev bound states in

- supercurrent-carrying carbon nanotubes revealed, *Nat. Phys.* **6**, 965 (2010).
- [18] L. Bretheau, Ç. Ö. Girit, C. Urbina, D. Esteve, and H. Pothier, Supercurrent Spectroscopy of Andreev States, *Phys. Rev. X* **3**, 041034 (2013).
- [19] B. van Heck, S. Mi, and A. R. Akhmerov, Single fermion manipulation via superconducting phase differences in multiterminal Josephson junctions, *Phys. Rev. B* **90**, 155450 (2014).
- [20] C. Padurariu, T. Jonckheere, J. Rech, R. Mélin, D. Feinberg, T. Martin, and Y. V. Nazarov, Closing the proximity gap in a metallic Josephson junction between three superconductors, *Phys. Rev. B* **92**, 205409 (2015).
- [21] T. Yokoyama and Y. V. Nazarov, Singularities in the Andreev spectrum of a multiterminal Josephson junction, *Phys. Rev. B* **92**, 155437 (2015).
- [22] R.-P. Riwar, M. Houzet, J. S. Meyer, and Y. V. Nazarov, Multi-terminal Josephson junctions as topological matter, *Nat. Commun.* **7**, 11167 (2016).
- [23] T. Yokoyama, J. Reutlinger, W. Belzig, and Y. V. Nazarov, Order, disorder, and tunable gaps in the spectrum of Andreev bound states in a multiterminal superconducting device, *Phys. Rev. B* **95**, 045411 (2017).
- [24] E. Eriksson, R.-P. Riwar, M. Houzet, J. S. Meyer, and Y. V. Nazarov, Topological transconductance quantization in a four-terminal Josephson junction, *Phys. Rev. B* **95**, 075417 (2017).
- [25] H.-Y. Xie, M. G. Vavilov, and A. Levchenko, Topological Andreev bands in three-terminal Josephson junctions, *Phys. Rev. B* **96**, 161406 (2017).
- [26] J. S. Meyer and M. Houzet, Nontrivial Chern Numbers in Three-Terminal Josephson Junctions, *Phys. Rev. Lett.* **119**, 136807 (2017).
- [27] H.-Y. Xie, M. G. Vavilov, and A. Levchenko, Weyl nodes in Andreev spectra of multiterminal Josephson junctions: Chern numbers, conductances, and supercurrents, *Phys. Rev. B* **97**, 035443 (2018).
- [28] E. V. Repin, Y. Chen, and Y. V. Nazarov, Topological properties of multiterminal superconducting nanostructures: Effect of a continuous spectrum, *Phys. Rev. B* **99**, 165414 (2019).
- [29] L. P. Gavensky, G. Usaj, and C. A. Balseiro, Topological phase diagram of a three-terminal Josephson junction: From the conventional to the Majorana regime, *Phys. Rev. B* **100**, 014514 (2019).
- [30] M. Houzet and J. S. Meyer, Majorana-Weyl crossings in topological multiterminal junctions, *Phys. Rev. B* **100**, 014521 (2019).
- [31] K. Sakurai, M. T. Mercaldo, S. Kobayashi, A. Yamakage, S. Ikegaya, T. Habe, P. Kotetes, M. Cuoco, and Y. Asano, Nodal Andreev spectra in multi-Majorana three-terminal Josephson junctions, *Phys. Rev. B* **101**, 174506 (2020).
- [32] R. L. Klees, G. Rastelli, J. C. Cuevas, and W. Belzig, Microwave Spectroscopy Reveals the Quantum Geometric Tensor of Topological Josephson Matter, *Phys. Rev. Lett.* **124**, 197002 (2020).
- [33] Y. Chen and Y. V. Nazarov, Spin-Weyl quantum unit: theoretical proposal, [arXiv:2008.06070](https://arxiv.org/abs/2008.06070).
- [34] V. Fatemi, A. R. Akhmerov, and L. Bretheau, Weyl Josephson Circuits, [arXiv:2008.13758](https://arxiv.org/abs/2008.13758).
- [35] M. Kolodrubetz, V. Gritsev, and A. Polkovnikov, Classifying and measuring geometry of a quantum ground state manifold, *Phys. Rev. B* **88**, 064304 (2013).
- [36] T. Neupert, C. Chamon, and C. Mudry, Measuring the quantum geometry of Bloch bands with current noise, *Phys. Rev. B* **87**, 245103 (2013).
- [37] P. Zanardi, P. Giorda, and M. Cozzini, Information-Theoretic Differential Geometry of Quantum Phase Transitions, *Phys. Rev. Lett.* **99**, 100603 (2007).
- [38] Y. Gao, S. A. Yang, and Q. Niu, Field Induced Positional Shift of Bloch Electrons and Its Dynamical Implications, *Phys. Rev. Lett.* **112**, 166601 (2014).
- [39] O. Bleu, G. Malpuech, Y. Gao, and D.D. Solnyshkov, Effective Theory of Nonadiabatic Quantum Evolution Based on the Quantum Geometric Tensor, *Phys. Rev. Lett.* **121**, 020401 (2018).
- [40] D. D. Solnyshkov, C. Leblanc, L. Bessonart, A. Nalitov, J. Ren, Q. Liao, F. Li, G. Malpuech, Quantum metric and wavepackets at exceptional points in non-Hermitian systems, [arXiv:2009.06987](https://arxiv.org/abs/2009.06987).
- [41] L. P. Gavensky, G. Usaj, D. Feinberg, and C. A. Balseiro, Berry curvature tomography and realization of topological Haldane model in driven three-terminal Josephson junctions, *Phys. Rev. B* **97**, 220505 (2018).
- [42] B. Venitucci, D. Feinberg, R. Mélin, and B. Douçot, Nonadiabatic Josephson current pumping by chiral microwave irradiation, *Phys. Rev. B* **97**, 195423 (2018).
- [43] N. Fläschner, B. S. Rem, M. Tarnowski, D. Vogel, D.-S. Lühmann, K. Sengstock, and C. Weitenberg, Experimental reconstruction of the Berry curvature in a Floquet Bloch band, *Science* **352**, 1091 (2016).
- [44] L. Asteria, D. T. Tran, T. Ozawa, M. Tarnowski, B. S. Rem, N. Fläschner, K. Sengstock, N. Goldman, and C. Weitenberg, Measuring quantized circular dichroism in ultracold topological matter, *Nat. Phys.* **15**, 449 (2019).
- [45] X. Tan, D.-W. Zhang, Q. Liu, G. Xue, H.-F. Yu, Y.-Q. Zhu, H. Yan, S.-L. Zhu, and Y. Yu, Topological Maxwell Metal Bands in a Superconducting Qutrit, *Phys. Rev. Lett.* **120**, 130503 (2018).
- [46] M. D. Schroer, M. H. Kolodrubetz, W. F. Kindel, M. Sandberg, J. Gao, M. R. Vissers, D. P. Pappas, A. Polkovnikov, and K. W. Lehnert, Measuring a Topological Transition in an Artificial Spin-1/2 System, *Phys. Rev. Lett.* **113**, 050402 (2014).
- [47] X. Tan, D.-W. Zhang, Z. Yang, J. Chu, Y.-Q. Zhu, D. Li, X. Yang, S. Song, Z. Han, Z. Li, Y. Dong, H.-F. Yu, H. Yan, S.-L. Zhu, and Y. Yu, Experimental Measurement of the Quantum Metric Tensor and Related Topological Phase Transition with a Superconducting Qubit, *Phys. Rev. Lett.* **122**, 210401 (2019).
- [48] P. Roushan, C. Neill, Y. Chen, M. Kolodrubetz, C. Quintana, N. Leung, M. Fang, R. Barends, B. Campbell, Z. Chen, B. Chiaro, A. Dunsworth, E. Jeffrey, J. Kelly, A. Megrant, J. Mutus, P. J. J. O'Malley, D. Sank, A. Vainsencher, J. Wenner, T. White, A. Polkovnikov, A. N. Cleland, and J. M. Martinis, Observation of topological transitions in interacting quantum circuits, *Nature* **515**, 241 (2014).
- [49] M. Yu, P. Yang, M. Gong, Q. Cao, Q. Lu, H. Liu, S. Zhang, M. B. Plenio, F. Jelezko, T. Ozawa, N. Goldman, S.-L. Zhang, and J.-M. Cai, Experimental measurement of the quantum geometric tensor using coupled qubits in diamond, *Nat. Sci. Rev.* **7**, 254 (2019).
- [50] A. Gianfrate, O. Bleu, L. Dominici, V. Ardizzone, M. De Giorgi, D. Ballarini, G. Lerario, K. W. West, L. N. Pfeiffer, D. D. Solnyshkov, D. Sanvitto, and G. Malpuech, Measurement of the quantum geometric tensor and of

- the anomalous Hall drift, *Nature* **578**, 381 (2020).
- [51] M. Wimmer, H. M. Price, I. Carusotto, and U. Peschel, Experimental measurement of the Berry curvature from anomalous transport, *Nat. Phys.* **13**, 545 (2017).
- [52] P. Kotetes, M. T. Mercaldo, and M. Cuoco, Synthetic Weyl Points and Chiral Anomaly in Majorana Devices with Nonstandard Andreev-Bound-State Spectra, *Phys. Rev. Lett.* **123**, 126802 (2019).
- [53] L. J. Geerligs, S. M. Verbrugh, P. Hadley, J. E. Mooij, H. Pothier, P. Lafarge, C. Urbina, D. Estève, and M. H. Devoret, Single Cooper pair pump, *Z. Phys. B: Condens. Matter* **85**, 349 (1991).
- [54] J. P. Pekola, J. J. Toppari, M. Aunola, M. T. Savolainen, and D. V. Averin, Adiabatic transport of Cooper pairs in arrays of Josephson junctions, *Phys. Rev. B* **60**, R9931(R) (1999).
- [55] M. Aunola and J. J. Toppari, Connecting Berry's phase and the pumped charge in a Cooper pair pump, *Phys. Rev. B* **68**, 020502(R) (2003).
- [56] R. Leone and L. Lévy, Topological quantization by controlled paths: Application to Cooper pairs pumps, *Phys. Rev. B* **77**, 064524 (2008).
- [57] P. A. Erdman, F. Taddei, J. T. Peltonen, R. Fazio, and J. P. Pekola, Fast and accurate Cooper pair pump, *Phys. Rev. B* **100**, 235428 (2019).
- [58] L. Peyruchat, J. Griesmar, J.-D. Pillet, and Ç. Ö. Girit, Transconductance quantization in a topological Josephson tunnel junction circuit, [arXiv:2009.03291](https://arxiv.org/abs/2009.03291).
- [59] E. Strambini, S. D'Ambrosio, F. Vischi, F. S. Bergeret, Y. V. Nazarov, and F. Giazotto, The  $\omega$ -SQUIPT as a tool to phase-engineer Josephson topological materials, *Nat. Nanotechnol.* **11**, 1055 (2016).
- [60] M. Amundsen, J. A. Ouassou, and J. Linder, Analytically determined topological phase diagram of the proximity-induced gap in diffusive n-terminal Josephson junctions, *Sci. Rep.* **7**, 40578 (2017).
- [61] S. R. Plissard, I. van Weperen, D. Car, M. A. Verheijen, G. W. G. Immink, J. Kammhuber, L. J. Cornelissen, D. B. Szombati, A. Geresdi, S. M. Frolov, L. P. Kouwenhoven, and E. P. A. M. Bakkers, Formation and electronic properties of InSb nanocrosses, *Nat. Nanotechnol.* **8**, 859 (2013).
- [62] A. W. Draelos, M.-T. Wei, A. Serebinski, H. Li, Y. Mehta, K. Watanabe, T. Taniguchi, I. V. Borzenets, F. Amet, and G. Finkelstein, Supercurrent flow in multi-terminal graphene Josephson junctions, *Nano Lett.* **19**, 1039 (2019).
- [63] N. Pankratova, H. Lee, R. Kuzmin, K. Wickramasinghe, W. Mayer, J. Yuan, M. G. Vavilov, J. Shabani, and V. E. Manucharyan, Multiterminal Josephson Effect, *Phys. Rev. X* **10**, 031051 (2020).
- [64] A. Levy Yeyati, J. C. Cuevas, A. López-Dávalos, and A. Martín-Rodero, Resonant tunneling through a small quantum dot coupled to superconducting leads, *Phys. Rev. B* **55**, R6137(R) (1997).
- [65] M. R. Buitelaar, W. Belzig, T. Nussbaumer, B. Babić, C. Bruder, and C. Schönberger, Multiple Andreev Reflections in a Carbon Nanotube Quantum Dot, *Phys. Rev. Lett.* **91**, 057005 (2003).
- [66] L. Hofstetter, S. Csonka, J. Nygård, and C. Schönberger, Cooper pair splitter realized in a two-quantum-dot Y-junction, *Nature* **461**, 960 (2009).
- [67] L. G. Herrmann, F. Portier, P. Roche, A. Levy Yeyati, T. Kontos, and C. Strunk, Carbon Nanotubes as Cooper-Pair Beam Splitters, *Phys. Rev. Lett.* **104**, 026801 (2010).
- [68] G. Fülöp, F. Domínguez, S. d'Hollosy, A. Baumgartner, P. Makk, M.H. Madsen, V.A. Guzenko, J. Nygård, C. Schönberger, A. Levy Yeyati, and S. Csonka, Magnetic Field Tuning and Quantum Interference in a Cooper Pair Splitter, *Phys. Rev. Lett.* **115**, 227003 (2015).
- [69] P. Recher, E. V. Sukhorukov, and D. Loss, Andreev tunneling, Coulomb blockade, and resonant transport of non-local spin-entangled electrons, *Phys. Rev. B* **63**, 165314 (2001).
- [70] D. Feinberg, Andreev scattering and cotunneling between two superconductor-normal metal interfaces: the dirty limit, *Eur. Phys. J. B* **36**, 419 (2003).
- [71] M. V. Berry, Quantal phase factors accompanying adiabatic changes, *Proc. R. Soc. A* **392**, 45 (1984).
- [72] M. Nakahara, *Geometry, Topology, and Physics* (Institute of Physics Publishing, Bristol, 2003).
- [73] T. Fukui, Y. Hatsugai, and H. Suzuki, Chern Numbers in Discretized Brillouin Zone: Efficient Method of Computing (Spin) Hall Conductances, *J. Phys. Soc. Jpn.* **74**, 1674 (2005).
- [74] M. Kolodrubetz, D. Sels, P. Mehta, and A. Polkovnikov, Geometry and non-adiabatic response in quantum and classical systems, *Phys. Rep.* **697**, 1 (2017).
- [75] T. Ozawa and N. Goldman, Extracting the quantum metric tensor through periodic driving, *Phys. Rev. B* **97**, 201117 (2018).
- [76] S.-C. Zhang and J. Hu, A Four-Dimensional Generalization of the Quantum Hall Effect, *Science* **294**, 823 (2001).
- [77] Y. E. Kraus, Z. Ringel, and O. Zilberberg, Four-Dimensional Quantum Hall Effect in a Two-Dimensional Quasicrystal, *Phys. Rev. Lett.* **111**, 226401 (2013).
- [78] H. M. Price, O. Zilberberg, T. Ozawa, I. Carusotto, and N. Goldman, Four-Dimensional Quantum Hall Effect with Ultracold Atoms, *Phys. Rev. Lett.* **115**, 195303 (2015).
- [79] T. Ozawa, H. M. Price, N. Goldman, O. Zilberberg, and I. Carusotto, Synthetic dimensions in integrated photonics: From optical isolation to four-dimensional quantum Hall physics, *Phys. Rev. A* **93**, 043827 (2016).
- [80] C. Chan and X.-J. Liu, Non-Abelian Majorana Modes Protected by an Emergent Second Chern Number, *Phys. Rev. Lett.* **118**, 207002 (2017).
- [81] S. Sugawa, F. Salces-Carcoba, A. R. Perry, Y. Yue, and I. B. Spielman, Second Chern number of a quantum-simulated non-Abelian Yang monopole, *Science* **360**, 1429 (2018).
- [82] M. Lohse, C. Schweizer, H. M. Price, O. Zilberberg, and I. Bloch, Exploring 4D quantum Hall physics with a 2D topological charge pump, *Nature* **553**, 55 (2018).
- [83] O. Zilberberg, S. Huang, J. Guglielmon, M. Wang, K. P. Chen, Y. E. Kraus, and M. C. Rechtsman, Photonic topological boundary pumping as a probe of 4D quantum Hall physics, *Nature* **553**, 59 (2018).
- [84] I. Petrides, H. M. Price, and O. Zilberberg, Six-dimensional quantum Hall effect and three-dimensional topological pumps, *Phys. Rev. B* **98**, 125431 (2018).
- [85] C. H. Lee, Y. Wang, Y. Chen, and X. Zhang, Electromagnetic response of quantum Hall systems in dimensions five and six and beyond, *Phys. Rev. B* **98**, 094434 (2018).
- [86] L. Lu, H. Gao, and Z. Wang, Topological one-way fiber

- of second Chern number, *Nat. Commun.* **9**, 5384 (2018).
- [87] H. Weisbrich, R. L. Klees, G. Rastelli, and W. Belzig, Second Chern Number and Non-Abelian Berry Phase in Topological Superconducting Systems, [arXiv:2008.08319](https://arxiv.org/abs/2008.08319)
- [88] M. K. Murray, Bundle Gerbes, *J. London Math. Soc.* **54**, 405 (1996).
- [89] G. Palumbo and N. Goldman, Revealing Tensor Monopoles through Quantum-Metric Measurements, *Phys. Rev. Lett.* **121**, 170401 (2018).
- [90] G. Palumbo and N. Goldman, Tensor Berry connections and their topological invariants, *Phys. Rev. B* **99**, 045154 (2019).
- [91] X. Tan, D.-W. Zhang, D. Li, X. Yang, S. Song, Z. Han, Y. Dong, D. Lan, H. Yan, S.-L. Zhu, and Y. Yu, Experimental Observation of Tensor Monopoles with a Superconducting Qudit, [arXiv:2006.11770](https://arxiv.org/abs/2006.11770).
- [92] M. Chen, C. Li, G. Palumbo, Y.-Q. Zhu, N. Goldman, and P. Cappellaro, Experimental characterization of the 4D tensor monopole and topological nodal rings, [arXiv:2008.00596](https://arxiv.org/abs/2008.00596).
- [93] M. Zgirski, L. Bretheau, Q. Le Masne, H. Pothier, D. Esteve, and C. Urbina, Evidence for Long-Lived Quasiparticles Trapped in Superconducting Point Contacts, *Phys. Rev. Lett.* **106**, 257003 (2011).
- [94] J. Dittmann and G. Rudolph, On a connection governing parallel transport along  $2 \times 2$  density matrices, *J. Geom. Phys.* **10**, 93 (1992).
- [95] O. Viyuela, A. Rivas, and M. A. Martin-Delgado, Uhlmann Phase as a Topological Measure for One-Dimensional Fermion Systems, *Phys. Rev. Lett.* **112**, 130401 (2014).
- [96] O. Viyuela, A. Rivas, S. Gasparinetti, A. Wallraff, S. Filipp, and M. A. Martin-Delgado, Observation of topological Uhlmann phases with superconducting qubits, *npj Quantum Inf.* **4**, 10 (2018).